Performance of the Signal Vacuum Cables of the Liquid Argon Calorimeter Endcap Cryostat Signal Feedthroughs

D. Axen[1], P. Birney[2,3], A. Dowling[3],
A.S. Dowling[2,3], M. Fincke-Keeler[3], T. Hodges[2,3], F. Holness[3],
T. Ince[3], R. Keeler[3], R. Langstaff[2,3], M. Lefebvre[3], M. Lenckowski[2,3],
J. Lindner[3], R. MacDonald[3], R. McDonald[3], E. Muzzeral[3],
P. Poffenberger[3], J. Van Uytven[3], G. Vowles[3,4], W. Wiggins[3]

Abstract

This note presents of brief summary of the design specification and the performance under test of the signal vacuum cables which are used in the signal feedthroughs of the ATLAS liquid argon calorimeter endcap cryostats.

[1]University of British Columbia, Vancouver, Canada
[2]TRIUMF, Vancouver, Canada
[3]University of Victoria, Victoria, Canada
[4]now at the University of Toronto, Toronto, Canada

1 Overview

Cryogenic systems with a large number of readout channels can face significant heat leakage into the cryostat through signal cables in the cryogenic feedthroughs. In the ATLAS liquid argon calorimeters, the signals of nearly 200,000 channels have to be read out. Such a large number of channels requires serious consideration of what kind of conductors are to be used to conduct signals between the cold and ambient vessels of the cryostat. Microstrip transmission lines have been chosen for the ATLAS liquid argon calorimeters in order to minimize the amount of conductive material while maintaining the integrity of the signals. These cables, referred to as vacuum cables, are installed inside an evacuated volume of the signal feedthroughs which provides an insulating interface between the cold and ambient flanges of the feedthroughs. A schematic diagram of a signal feedthrough is shown in Figure 1. There are 30 vacuum cables in each feedthrough, and each cable carries 64 signals.

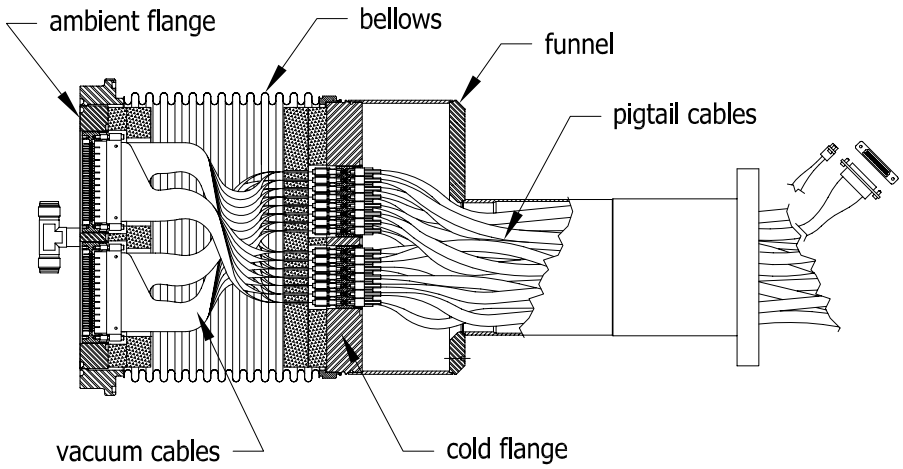

Figure 1: A schematic of a signal feedthrough, showing the vacuum cables and several other major components.

There are 25 signal feedthroughs on each endcap cryostat. The primary design criterion for the vacuum cables is to achieve low thermal conduction to the cryogenic system while still maintaining faithful and reliable signal propagation. The proposal to use stripline cables and the initial design parameters of the cables came from the Brookhaven National Laboratory. Performance requirements of these cables were outlined in reference [1] before tender, leading to a formal request for quotes and awarding of the contract to FCI Electronics. The low voltage (LV) vacuum cables of the *HEC* feedthroughs are not discussed in this note; design specifications for those cables may be found in reference [2].

2 Physical Description

The signal vacuum cables, shown schematically in Figure 2, are 34.9 cm from face to face. Each vacuum cable consists of two mirror-symmetric striplines. The striplines each consists

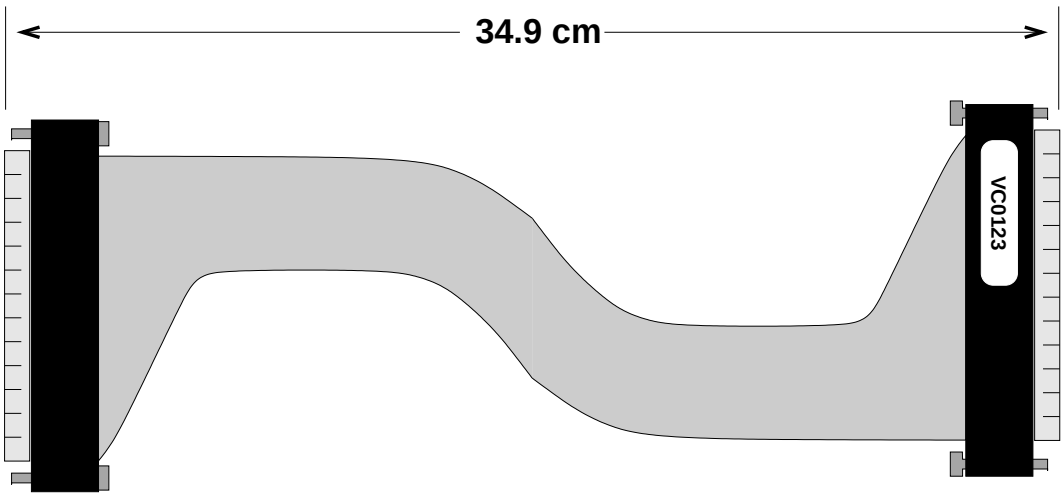

Figure 2: A schematic of an endcap signal feedthrough vacuum cable.

of 32 transmission lines, with each transmission line consisting of a copper signal trace and a copper ground trace separated by 51 μm polyimide dielectric[1]. The nominal widths of the signal and ground traces are 204 μm and 357 μm respectively, while the nominal thickness is 34 μm for each. The manufacturer, however, was allowed to make minor adjustments to these dimensions in order to meet the impedance and resistance requirements. Both signal and ground traces are covered with 76 μm of polyimide and adhesive[2]. The two striplines of each vacuum cable are arranged such that the signal traces face each other on the inside and the ground traces are facing the outside. A schematic cross section of a section of the stripline is shown in Figure 3.

The connectors at each end of the vacuum cable have 64 gold-plated sockets arranged in a 2×32 configuration, 2.54 mm spacing, for mating the 64 signal traces to the 64 pins of a pincarrier in the cold or ambient flange. The ground traces are connected to the pincarrier by gold-plated ground shields on either side of each connector. The 32 ground traces of each stripline are common to the connector ground shields on the corresponding side of the connector, however the grounds on each side of the connector, and hence of the two striplines, are isolated from each other.

[1] DuPont AP9121 Copper-Clad Laminate
[2] DuPont LF0120 Pyralux LF Coverlay

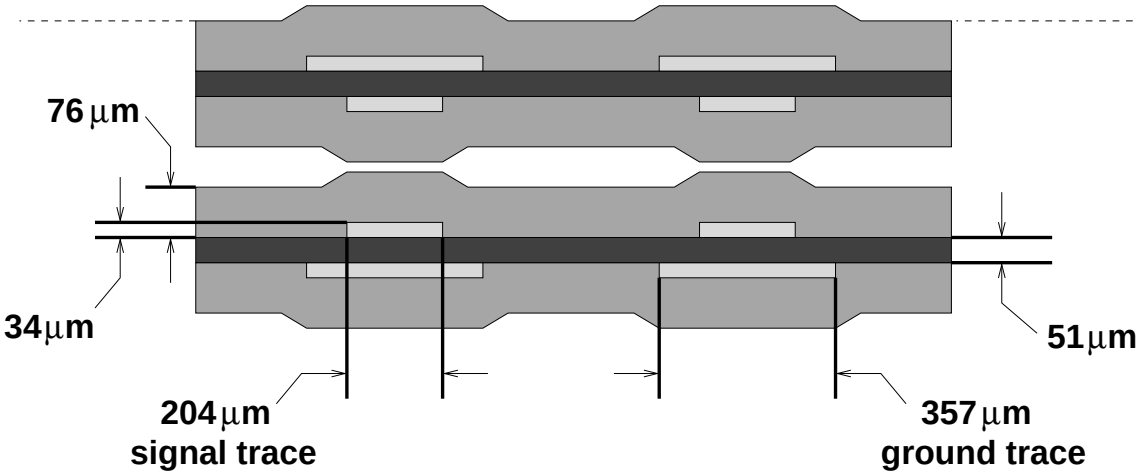

Figure 3: A schematic cross section of the vacuum cable striplines. All dimensions shown are nominal.

3 Frequency Dependent Measurements and Modeling

A typical ATLAS LAr pulse has a rise time of approximately 20 ns, corresponding to a bandwidth of 17.5 MHz. Frequency dependent measurements up to 50 MHz of the characteristic parameters of a vacuum cable are therefore adequate to describe its performance in ATLAS.

3.1 Measurements

In order to study the frequency dependent behaviour of a vacuum cable, the complex impedance of the stripline has been measured with a network analyzer [3] in terms of its magnitude ($|Z|$) and phase (ϕ). This measurement has been performed with both open ($|Z_{oc}|, \phi_{oc}$) and short ($|Z_{sc}|, \phi_{sc}$) termination of the stripline [4]. Given the magnitude and phase, the complex quantities Z_{sc} and Z_{oc} can be constructed. Using the high frequency TEM mode approximation, it is possible to calculate characteristic stripline parameters from these measurements [5].

The characteristic impedance(Z_o) and the quantity $\tanh(\gamma l)$ are given by

$$Z_o = \sqrt{Z_{sc} Z_{oc}}\ , \tag{1}$$

$$\tanh(\gamma l) = \sqrt{Z_{sc}/Z_{oc}}\ , \tag{2}$$

where l is the length of the stripline and γ is the propagation coefficient $\gamma = \alpha + i\beta$, where α is the attenuation coefficient and β the phase-change coefficient of the cable. For a typical vacuum cable, the measured characteristic impedance as a function of frequency (up to

[3] Network analyzer hp8735B in combination with with a hp85047A S-Parameter set.

[4] These measurements were performed on a preproduction cable. The impedance of the preproduction batch was slightly higher than the impedance of the final production.

[5] See for example: T.C.Edwards "Foundations for Microstrip Circuit Design" John Wiley & Sons 1981.

50 MHz) is shown in Figure 4. For an electrical length of the stripline of 41 cm (including the connectors and terminator), the measured frequency dependence of the attenuation is shown in Figure 5.

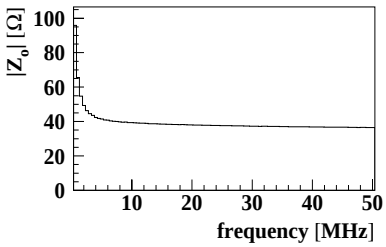

Figure 4: Characteristic impedance measured as a function of frequency.

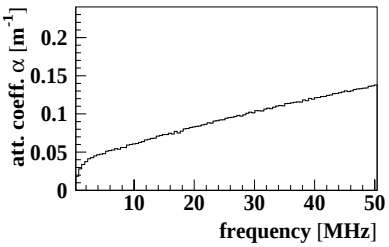

Figure 5: Attenuation coefficient measured as a function of frequency.

Based on the measured quantities, the resistance, inductance, conductance and capacitance (per unit length) of the stripline can also be determined:

$$R = \Re e(\gamma\sqrt{Z_{sc}Z_{oc}}) \ , \tag{3}$$

$$L = \Im m(\gamma\sqrt{Z_{sc}Z_{oc}})/2\pi\nu \ , \tag{4}$$

$$G = \Re e(\gamma/\sqrt{Z_{sc}Z_{oc}}) \ , \tag{5}$$

$$C = \Im m(\gamma/\sqrt{Z_{sc}Z_{oc}})/2\pi\nu \ . \tag{6}$$

The frequency (ν) dependence (up to 50 MHz) of these parameters is shown in Figure 6.

These parameters allow a calculation of the phase velocity,

$$v_p = \frac{1}{\sqrt{LC}} = \frac{1}{\sqrt{\mu\epsilon}} \ . \tag{7}$$

Since the permeability of copper is $\mu_r \approx 1$, the phase velocity depends entirely on the relative dielectric constant ϵ_r. Using the values of L and C calculated from the measurements, v_p and ϵ_r can be determined. Their frequency dependence is shown in Figures 7 and 8. At a phase velocity of 1.6×10^8 m/s, the propagation delay of a 40 cm long stripline is 2.5 ns, which is in good agreement with the time domain reflectometry (TDR) measurements which are shown in Figure 16(a). The section of the trace that represents the vacuum cable is limited by two strong peaks, which are caused by the connectors at either end of the cable. The time between the two peaks is twice the delay time of a vacuum cable.

3.2 Theoretical Description of the Stripline

Laplace's equation was solved numerically to obtain the electric field for a given conductor geometry. Applying Gauss' law then yields the capacitance per unit length. This technique allows a study of the effects of the variation of the stripline geometry and the effects of possible variations of the values of the material properties. Such variations can arise from

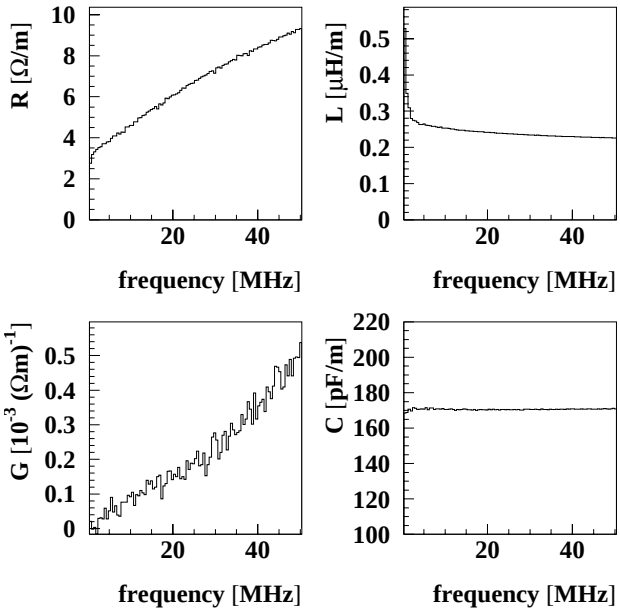

Figure 6: Resistance, inductance, conductance and capacitance per unit length as a function of frequency, determined from measurements.

the production process, which limits the accuracy on the width of the strips to about ± 10 μm. The relative dielectric constant ϵ_r varies with frequency, temperature, and humidity; for polyimide its value can range typically from 3.2 to 3.5, with its nominal value given to be 3.2 [6].

The general layout of the stripline has been described in section 3. The geometry used for the solution of Laplace's equation assumes that the conductive strips are separated vertically by a 50 μm thick layer of polyimide. A 50 μm thick outer polyimide layer is attached to the stripline with an adhesive. For simplicity, the adhesive is assumed to fill the lateral gap between the conductive strips with a thickness that is the same as the strip thickness (see Figure 9).

The following parameters have been varied: the widths and thicknesses of the signal and ground strips, and the relative dielectric constant of polyimide and the adhesive material [7]. In addition, a misalignment between the signal and ground strips can be taken into account.

For each possible geometry Laplace's equation has to be solved twice, once for the case that the copper conductors are surrounded by vacuum and once for the case with polyimide and adhesive material present. The results yield two capacitances, C_v and C_ϵ respectively.

[6] See data sheets on: http://www.dupont.com/kapton.

[7] No specific value is given in the data sheets for the adhesive alone, but specifications for dielectrics that give an average dielectric constant for polyimide and adhesive indicate that the dielectric constant of the adhesive alone is larger than that of the polyimide.

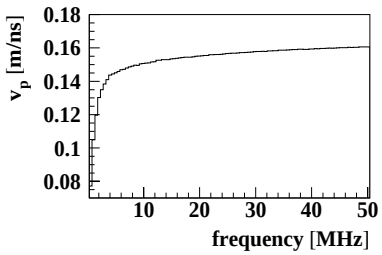

Figure 7: Phase velocity as a function of frequency.

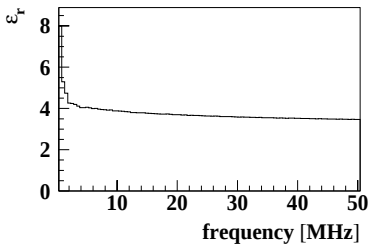

Figure 8: Relative dielectric constant as a function of frequency.

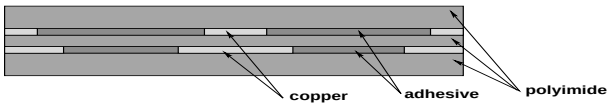

Figure 9: Schematic geometry layout for the numerical treatment of Laplace's equation.

The characteristic impedance can then be determined from:

$$Z_o = \frac{1}{c^2\sqrt{C_v C_\epsilon}} \ . \tag{8}$$

Table 1 lists the results of the calculations for various strip sizes and dielectric constants. It can be seen that the expected variations do not impact the performance of the vacuum cable significantly. The values of the impedance caused by the different variations of the geometry and material properties have a spread of approximately 4 Ω, which is in agreement with the width of the distribution of the measured impedances shown in Figure 16(b).

Given the capacitances as calculated from the solution of Laplace's equation, for vacuum (C_v) and Polyimide/adhesive (C_ϵ) as dielectric, it is possible to determine the characteristic cable parameters. In the high frequency approximation, the inductance is

$$L = 1/(c^2 C_v) \ . \tag{9}$$

The resistance per unit length can be calculated as the resistivity of copper (1.72 $\mu\Omega$ cm) divided by the geometric cross section of the stripline conductors. The skin effect has to be taken into account in this calculation. For simplicity, we have assumed that the signal strip is fully penetrated when the skin depth δ is larger than half the thickness of the signal strip. For δ smaller than half the thickness of the signal strip, a band of thickness δ along the outer cross section of the signal strip is assumed to be homogeneously penetrated. The penetration depth of the ground strip is assumed to drop off exponentially, starting from the side of the ground strip that faces the signal strip. With these assumptions, the magnitude of the propagation constant can be calculated as

$$|\gamma|^2 = \gamma^* \gamma \ , \tag{10}$$

	signal width (μm)	ground width (μm)	strip thickness (μm)	ϵ_r polyimide	ϵ_r adhesive	C_v (pF/m)	C_ϵ (pF/m)	Z_o (Ω)
a	200	360	34	3.2	4.0	51.4	172.5	35.4
b	200	360	34	3.4	4.0	51.4	182.4	34.4
c	200	360	34	3.2	4.4	51.4	174.1	35.4
d	200	360	30	3.2	4.0	51.0	171.8	35.6
e	190	360	34	3.2	4.0	49.7	167.6	36.5
f	180	360	34	3.2	4.0	48.3	162.4	37.6
g	180	315	34	3.2	4.0	47.2	158.8	38.5
h	220	385	34	3.2	4.0	55.0	171.8	34.3
i	200 ($\rightarrow$)	360	34	3.2	4.0	51.2	172.1	35.5

Table 1: Values of C_v, C_ϵ and Z_o based on the numerical solution of Laplace's equation for various stripline geometries. Case **a** represents the nominal geometry. In case **i**, the arrow implies that there is a misalignment of 20 μm between the signal trace and the ground trace.

with

$$\gamma = \sqrt{(R + i\omega L)(i\omega C)} \; . \tag{11}$$

The conductance G is very small compared to ωC and can be neglected in this case. The impedances for open and short circuit termination now become

$$Z_{oc} = Z_o \cdot \coth(\gamma l_{oc}) \; , \tag{12}$$

$$Z_{sc} = Z_o \cdot \tanh(\gamma l_{sc}) \; , \tag{13}$$

where l_{oc} and l_{sc} are the electrical lengths of the stripline with open circuit and short circuit termination respectively. It is now possible to calculate all the other stripline parameters as a function of frequency. Figure 10 shows a comparison of the measured values (solid line) of Z_o, R, C and α with the theoretical prediction for the vacuum cable (dashed line), given by case **a** of Table 1. This comparison extends up to 100 MHz. The quarter wavelength range for the cable is reached at that point, resulting in a peak of the distributions due to a small difference in the electrical lengths of the measurements with open circuit and short circuit termination. In this case this difference has been modeled with a length of 40.2 cm for the open circuit case and 41.4 cm for the short circuit case.

The results of the theoretical calculations are in good agreement with the measurements. The differences between the calculation and the data can be attributed to the high frequency TEM mode approximation, the simplified treatment of the skin effect and the uncertainty in dielectric parameters. It should be noted at this point that the connectors of the vacuum cable cannot be easily modeled, but do have an impact on the performance. Nevertheless, the level of agreement is more than adequate to evaluate the effects of various stripline parameters.

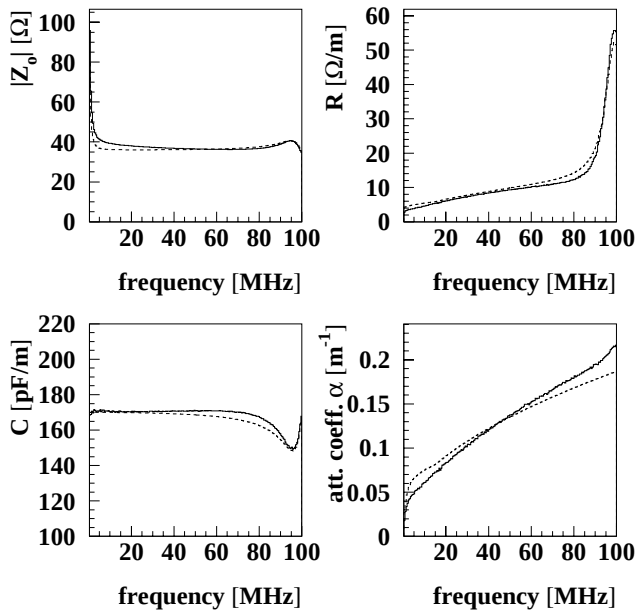

Figure 10: Comparison of Z_o, R, C and α as determined from measurement (solid line) with the theoretical prediction of case **a** of Table 1 (dotted line).

4 Electrical Tests

Each vacuum cable was subjected to a number of electrical tests on reception. These tests are outlined below. All vacuum cables which did not pass the reception tests were returned to the supplier for repair.

4.1 Cross talk

The primary motivation for measuring the cross talk is to find possible discontinuities in the ground traces, since the cross talk of the *adjacent* nearest-neighbor is considerably enhanced if such a fault occurs (see Figure 11). It should be noted that cross talk measured for the *opposite* nearest neighbor does not yield any information regarding the integrity of the ground traces, since the grounds of the two striplines are electrically isolated from each other. The cross talk of the nearest neighbor on the *opposite* stripline is nonetheless measured in order to detect possible shorts that may occur between signal traces within the connectors.

A schematic of the apparatus used to measure the cross talk is shown in Figure 12. Pulses are generated with a BNC Model BL-2 pulse generator, set to *tail pulse* mode, with exponential rise and decay times of 3 ns and 100 ns respectively. A typical signal from the pulse generator is shown in Figure 13(a). A fanout operated under computer control directs the pulses in succession to each of the 64 channels of the vacuum cable under test. A scanner, also under computer control, reads out the signals from the pulsed channel and from each of the nearest neighbors. The connections between the fanout, vacuum cable, and scanner are

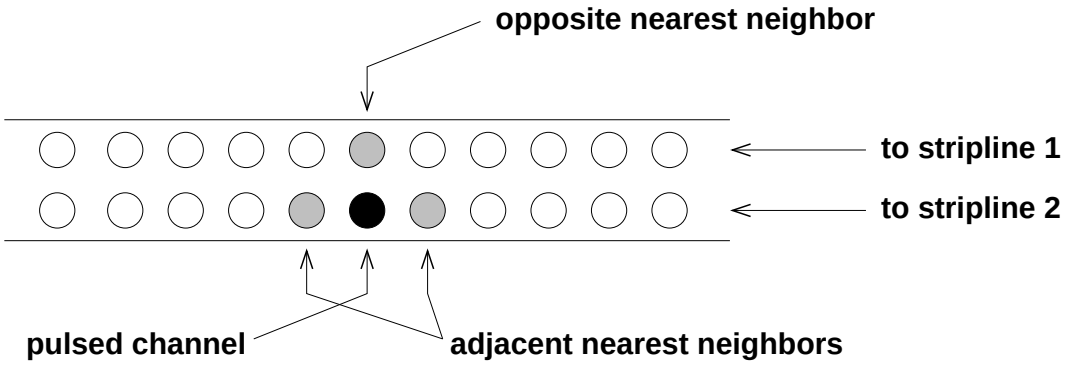

Figure 11: A cross sectional schematic of a vacuum cable, showing how the adjacent and nearest neighbors are chosen for the cross talk tests.

made with pigtail cables and pincarriers of the type used for the ATLAS signal feedthroughs. All pulses are amplified and shaped, using a $CRRC2$ circuit similar to the one to be used in ATLAS, before being digitized and stored on a computer. Typical shaped and amplified pulses from a pulsed channel and from nearest neighbors to the pulsed channel are shown in Figures 13(b), 13(c), and 13(d). Note that the pulses shown in Figures 13(c) and 13(d) include cross talk contributed from the two interconnecting pigtail cables in addition to the vacuum cable under test.

The percent cross talk is simply calculated as:

$$100 \times \frac{peak-to-peak\ amplitude\ of\ cross\ talk\ signal}{peak-to-peak\ amplitude\ of\ pulsed\ signal} \ .$$

Histograms of percent cross talk from a sample of 580 vacuum cables are shown in Figure 14. The mean cross talk for adjacent nearest neighbors, Figure 14(a), is 0.23%, while the mean cross talk for opposite nearest neighbors, Figure 14(b), is 0.69%. Cross talk of the opposite nearest neighbor has a larger range due to the capacitive coupling between the signal strips which lie against one another for opposite nearest neighbors, the magnitude of which depending on how precisely aligned are the two striplines. Note that the cross talk shown in Figure 14 is corrected for the contribution from the interconnecting pigtail cables, the previously measured percent cross talk from the pigtails being subtracted from the measured cross talk of the pigtail and vacuum cable combination.

Discontinuous ground traces were identified by the cross talk tests in a total of three out of 1750 vacuum cables. Opposite channel shorts were also identified in two vacuum cables from this test.

4.2 Signal Trace Resistance and Continuity

The resistance of each signal trace is measured with a Keithley model 580 micro-ohmmeter, which uses a four-wire measuring technique for high precision. The micro-ohmmeter was operated in single trigger and pulse mode, with the range set to 20 Ω. The vacuum cables were each connected to a 64 channel multiplexer which was designed and built for the

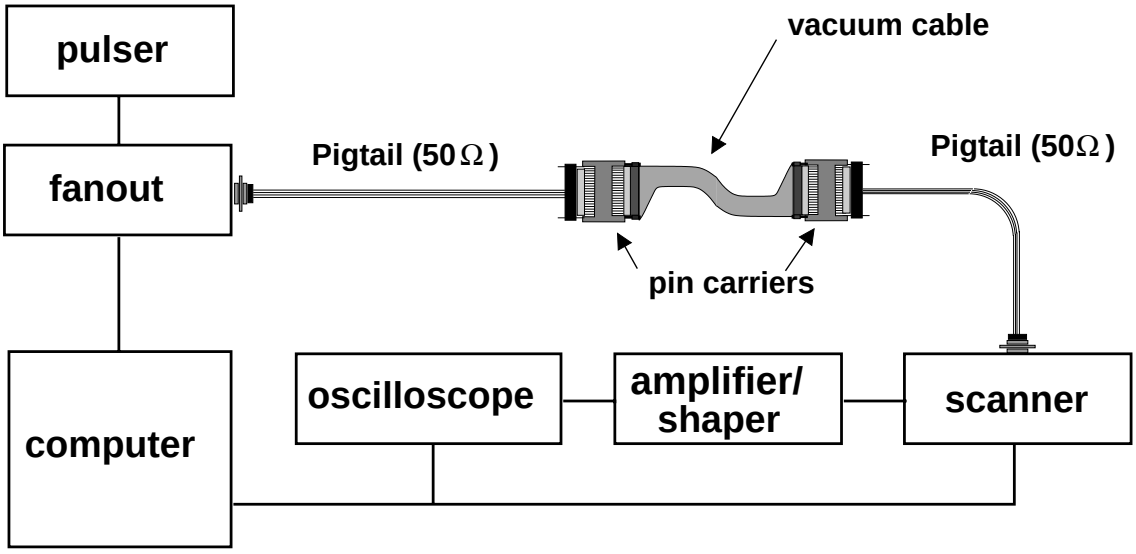

Figure 12: A schematic of the apparatus used to measure cross talk in the vacuum cables of the ATLAS endcap signal feedthroughs.

measurement. The lead resistance of the multiplexer is negligible (< 1 mΩ). Both the micro-ohmmeter and the multiplexer were under computer control, with each measurement being stored on disk. A typical resistance plot is shown in Figure 15(a). Note the two resistance bands corresponding to the differing trace resistances of the two striplines. A histogram of resistances for a sample of 574 vacuum cables is shown in Figure 15(b).

The specification for trace resistance of most vacuum cables is not particularly stringent, $0.6\ \Omega < R < 1.2\ \Omega$. However, those vacuum cables which are to be used for calibration channels (slots 15 of the *Standard* feedthroughs and slots 3 and 4 of the *HEC* feedthroughs[3]) demand much tighter tolerances to maintain uniform attenuation over a particular feedthrough. The trace resistances of the vacuum cables corresponding to the calibration channels were required to fall within a band of 50 mΩ for each feedthrough which contains calibration channels. Note that the absolute magnitude of the 50 mΩ resistance band is not important; the trace resistances of the calibration cables in different feedthroughs may differ significantly, it is only within a given feedthrough that the trace resistances of the calibration cables must all be within 50 mΩ of each other. The precision resistance measurements allowed those vacuum cables which met this requirement to be identified and set aside for use in the calibration channels. There was no difficulty in assembling a sufficient number of pairs of vacuum cables for the *Standard* feedthroughs or quartets of vacuum cables for the *HEC* feedthroughs where all trace resistances of each pair or quartet fell within a 50 mΩ band.

Each vacuum cable is also tested for signal trace continuity using a Cirris Touch I cable tester, operated in *continuous* mode. While being tested, the striplines of the cable are gently wiggled, so that any intermittent continuity fault in the signal traces might be found. Abnormally high resistance or opens were found in a total of thirteen out of 1750 vacuum cables.

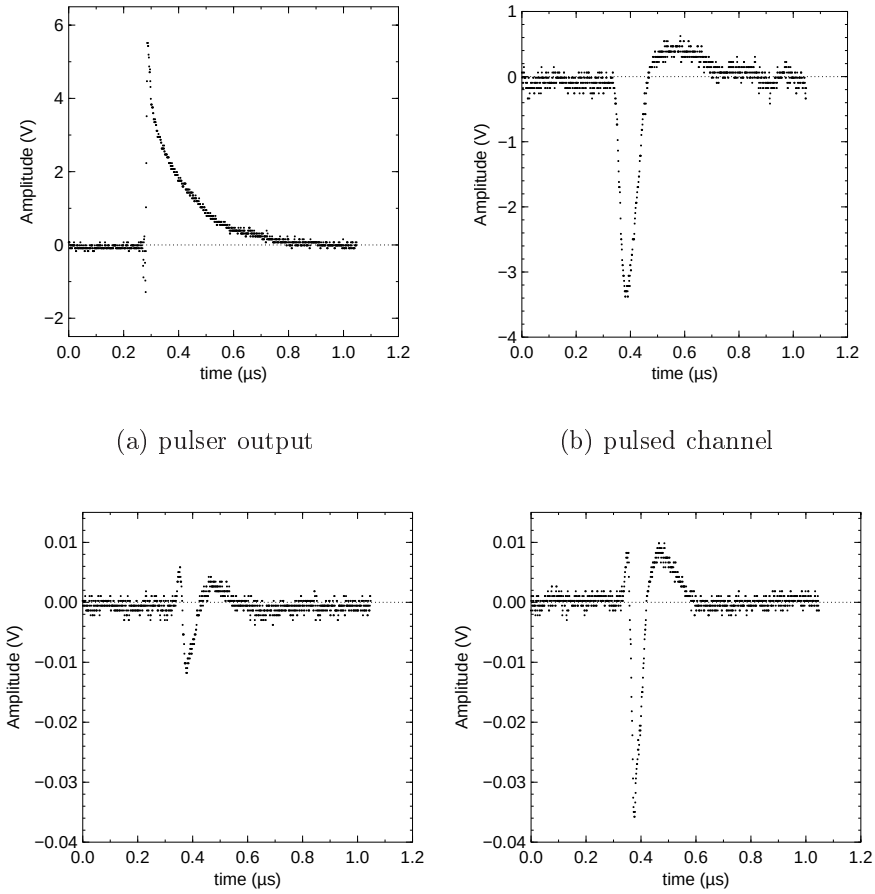

(a) pulser output

(b) pulsed channel

(c) adjacent channel

(d) opposite channel

Figure 13: A sample signal from the pulser output before amplification and shaping is shown in (a), and after amplification and shaping in (b). Signals from an adjacent and opposite neighbor after amplification and shaping are shown in (c) and (d) respectively.

4.3 Impedance

The impedance of six representative striplines was measured for each vacuum cable using a Hewlett Packard 8735B network analyzer, with a Hewlett Packard 85047A S-Parameter set operating in the 300 kHz to 3 GHz range. The network analyzer was operated in a time-domain low-pass step mode, with *minimum* windowing (essentially no windowing) and 801 points (frequency samples). For each vacuum cable, the impedance of three transmission lines was measured on each of the two striplines. The six lines measured correspond to ATLAS signal channels 1, 14, 25, 40, 51, and 64[3]. Data acquisition was under computer control, using a Hewlett Packard 8769K microwave switch with 18 GHz bandwidth to switch among the six channels, and a LabView VI to control the network analyzer and microwave switch and store the data collected onto the computer. A 50 Ω coaxial line was used to connect the multiplexer to the network analyzer, and the measured lines were each terminated with

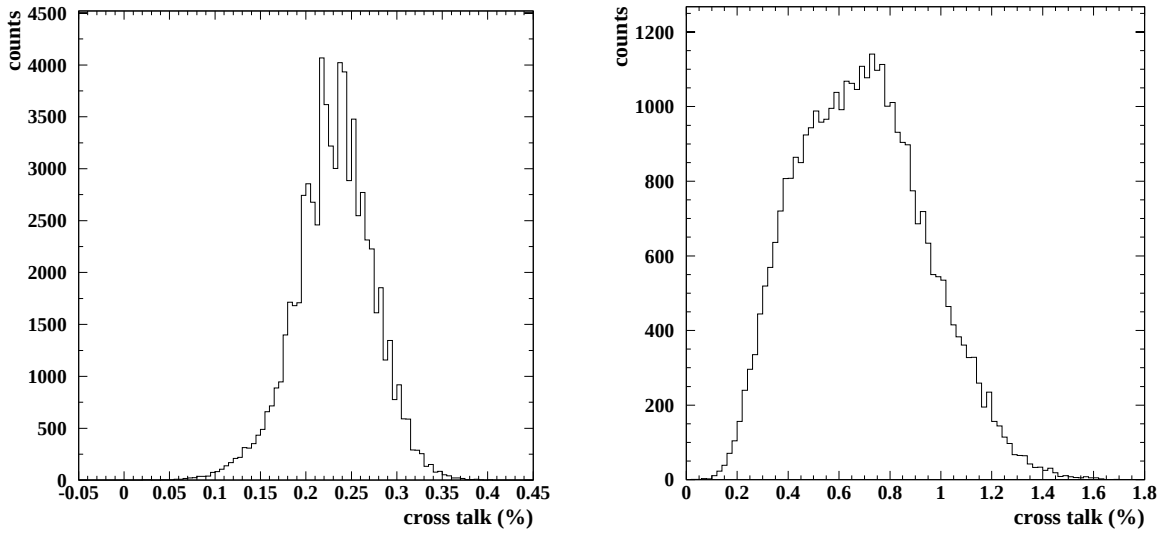

(a) adjacent neighbors

(b) opposite neighbors

Figure 14: Histograms of percent cross talk from a sample of 580 vacuum cables for adjacent neighbors (a) and for opposite neighbors (b).

precisely measured 33 Ω resistors to help provide a calibration for the system. One sample trace (Time Domain Reflectometry plot) is shown in Figure 16(a). The transmission line of the vacuum cable is that part of the plot lying in the 8 ns to 11 ns range. A histogram of measured impedances from a sample of 575 vacuum cables is shown in Figure 16(b). Note that the 32.9 Ω mean of the distribution of measured impedances is close to the nominal 33 Ω. A vacuum cable was considered failed and not used if the average measured impedance of the three lines of either stripline fell outside the range $28\ \Omega < Z < 38\ \Omega$. Only one vacuum cable out of 1750 did not meet the impedance specifications.

4.4 Ground Shield Contact Resistance

Measurements are also made in order to verify good electrical contact between the ground shields of a vacuum cable and a pincarrier, and also between a ground shield on one end of a vacuum cable with the ground shield on the opposite end. This test was designed to detect flat, bent, or otherwise defective ground shields, as well as poor electrical contact between the ground shield and the ground traces of the stripline.

A measuring apparatus with two fake pincarrier sockets was designed and built for this test. The ground shields of the vacuum cables are each divided into 13 segments, and so contact the pincarrier socket at 13 different points at each side of each connector. The fake pincarrier sockets of the test apparatus have two gold plated contacts for each of the ground shield segments, thus allowing a precise four-wire resistance measurement between one segment of one ground shield and the corresponding segment of the ground shield at the opposite end (but same side) of the cable. A Keithley model 580 micro-ohmmeter connected to the apparatus was used to perform the actual resistance measurement. The

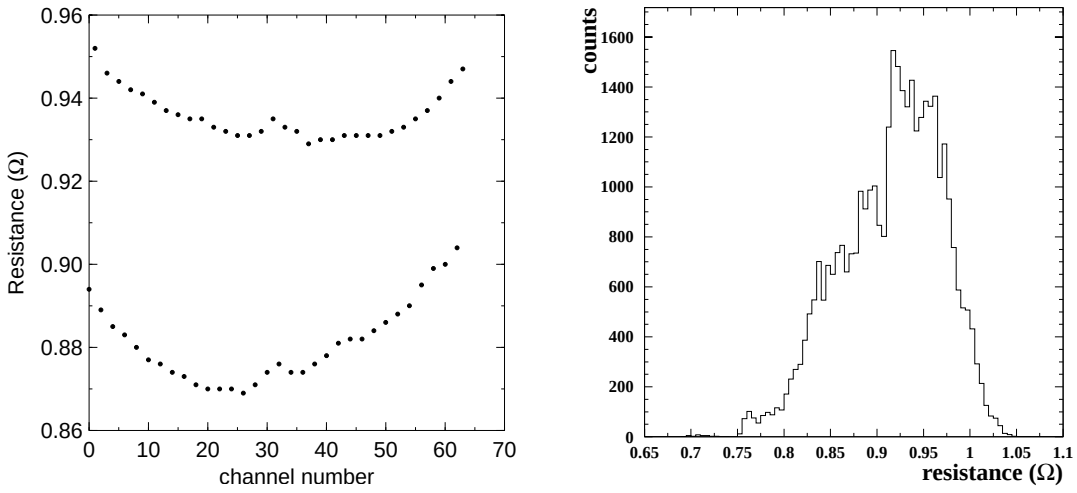

(a) resistance vs channel number

(b) histogram of resistances

Figure 15: A typical resistance plot for one vacuum cable is shown in (a). A histogram of measured trace resistances from a sample of 574 vacuum cables is shown in (b).

measuring apparatus is multiplexed, under computer control, so that the measurements of the 13 segments of each side of the cable can be stepped through and recorded, for a total of 26 contact resistance measurements for each cable. A histogram of measurements for a sample of 575 vacuum cables is shown in Figure 17.

Any vacuum cable having an abnormally high resistance (> 20 mΩ) or an open for more than two consecutive ground shield segments, or more than three segments in total on a ground shield, was considered failed and not used in the feedthroughs. A total of thirteen out of 1750 vacuum cables were failed for insufficient ground shield contact.

4.5 Other Observations

Apart from the electrical tests, there were a number of vacuum cables which were rejected due to mechanical problems with the connectors. The packing of the vacuum cable connectors into the pincarriers in the cold or ambient flanges is very tight, so that a connector which is over the tolerance in its width dimension is difficult or impossible to plug into a pincarrier. A number of cables arrived with one or both connectors over width, nine being sufficiently over width to return to the supplier for repair.

An integral part of the connector is a plastic spacer which is located within the connector and separating the two striplines. The spacer is held in place by a pin, off centre in the axial direction. This spacer was installed inverted in 96 vacuum cables, such that it protruded several millimeters outside the connector, consequently leaving additional area inside the connector unprotected against potential shorts between the two striplines (see below). One cable arrived with the centre spacer missing altogether. All these cables were returned for repair.

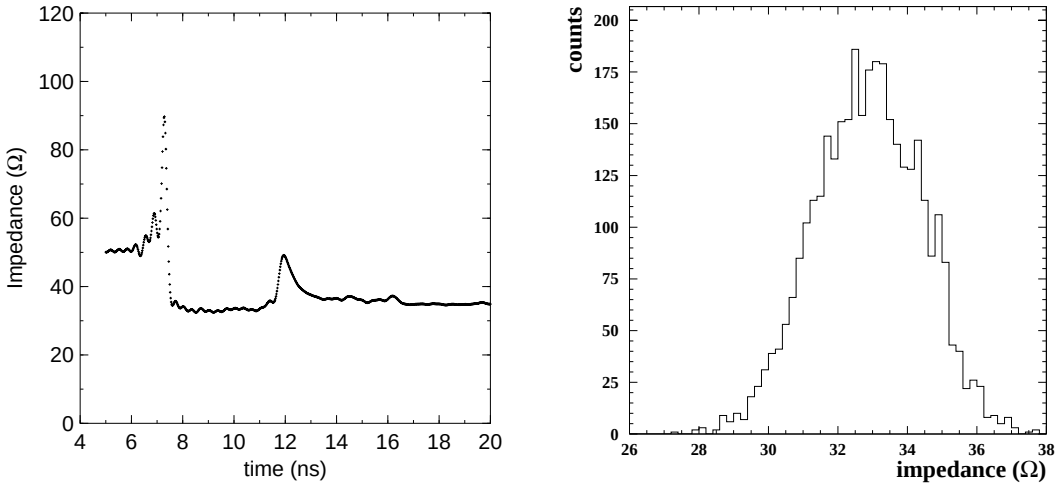

(a) typical TDR plot

(b) histogram of impedances

Figure 16: A typical TDR plot for one channel of a vacuum cable is shown in (a). A histogram of measured impedances from a sample of 575 vacuum cables is shown in (b).

There is an unfortunate feature of the connector design which allows for the possibility of shorts between opposite channels. On each end of the striplines are solder pads, onto which the pin sockets are soldered. Since the signal traces of the two striplines face each other (see Figure 3) the two solder pads at each end of the cable also face each other. These solder pads are contained within the connectors. Most, but not all, of the area of each solder pad is physically blocked from touching the adjacent solder pad by the centre spacer and other internal parts of the connector. If the soldering has been poorly done, or if the stripline is crinkled when installed into the connector, shorts can occur between opposite channels at the solder pad. Since there are unpredictable stresses and movements within the connector when plugged into a pincarrier, these shorts sometimes depend on exactly which pincarrier into which the cable is plugged or how deeply the cable is seated. More troublesome is that there is further movement within the connector under cold conditions, so that a cable which behaves fine under ambient conditions might fail during the cold tests. Unfortunately, a fault discovered during a cold test necessitates the reopening of the feedthrough for replacement of the faulty vacuum cable. Attempts to reproduce the problem, using vacuum cables with known faults, with bench tests using cryogenic (LN2) temperatures, high voltages up to 1000 V, or a combination of both proved to be unreliable. The only reliable check was the cold test of a completed feedthrough.

Only two such shorts were found during reception testing. Seven more vacuum cables were found during construction of the 55 feedthroughs to have opposite-channel shorts, and a further four were found during cold tests of the feedthroughs. The four found during cold tests necessitated the reopening of the feedthrough to replace the faulty cables. Most of the failures were isolated to a single batch of 438 cables that arrived in November 2000.

Procedures[4] have been worked out to identify the faulty cables at the earliest possible

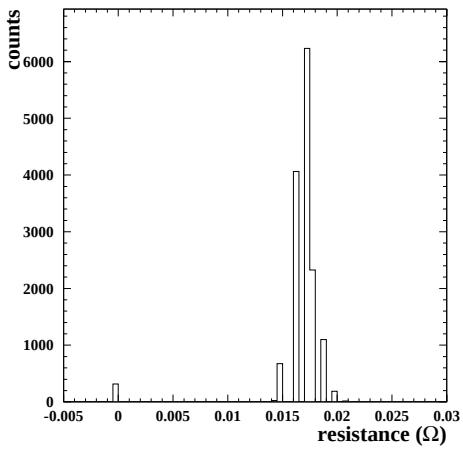

Figure 17: Histogram of resistance between ground shields on either end of the cable, taken from a sample of 575 vacuum cables. Those measurements which resulted in an open (∞ Ω) were recorded as 0 Ω.

stage of feedthrough assembly. As each vacuum cable is plugged into a pincarrier slot, it is checked for continuity, shorts to ground, and cross channel shorts, including a 100 V *HIPOT* test to detect *near* shorts. During the cool down of the feedthroughs for the final cold electrical tests, the vacuum cables are continuously monitored for opposite-channel shorts. One cable was found to have an opposite-channel short only at a temperature intermediate to ambient and cryogenic conditions; it showed no fault at either room temperature or LN2 temperature. We feel that through the procedures and careful steps which have been taken, most if not all the vacuum cables with opposite-channel shorts have been identified and replaced. A summary of the opposite-channel shorts and other modes and numbers of failures identified is presented in Table 2.

mode of failure	number of failures
high cross talk	3
opposite channel shorts (*vacuum cable reception tests*)	2
opposite channel shorts (*feedthrough construction and cold tests*)	11
high resistance or open	13
impedance out of tolerance	1
defective ground shield	13
connector width over tolerance	9
center spacer inverted	96
missing centre spacer	1

Table 2: The various failure modes and numbers of failures out of 1750 vacuum cables.

5 Conclusions

The signal vacuum cables used in the liquid argon calorimeter endcap cryostat signal feedthroughs have been put through a thorough set of electrical tests to ensure that each performs as required. The electrical characteristics of the vacuum cable striplines have proven to be very good, easily meeting the requirements of the ATLAS feedthroughs. The vacuum cable connectors have been more problematic, with weaknesses in both design and quality control during manufacture. Steps have been taken, however, to identify and remove those cables with faults.

The raw data from the cross talk, signal trace resistance, impedance, and ground contact resistance measurements are all viewable on the web. That data, along with other data relevant to the construction and testing of the feedthroughs can be found by following the links:

http://particle.phys.uvic.ca/~web-atlas/atlas/feedthroughs/status/
⇒ **ft***xx*
⇒ A summary ... can be found **here**.
⇒ vc*xxxx*

6 Acknowledgments

The authors acknowledge the invaluable contributions made to the design and procurement of the vacuum cables by the BNL Instrumentation Division under the direction of Veljko Radeka and the BNL Omega Physics group led by David Lissauer. The authors also wish to acknowledge the very helpful assistance of Gerald Oakham and Ernie Neuheimer of CRPP Carleton in the early design stages of the vacuum cables. Many positive features developed in these prototype cables found their way into the final design. We wish also to acknowledge the assistance of Christophe de la Taille, Nathalie Seguin, Pierre Imbert, and Emmanuel Collet of LAL Orsay in the development of the cross talk test apparatus, and also the contribution of the printed circuit board for that apparatus. Finally, we wish to acknowledge the help of Domenic Di Tomaso, Tom Felton, and Stan Knotek of the UBC Physics electronics shop for their contributions to the design and construction of the cross talk test apparatus, and Neil Honkanen of the UVic Physics electronics shop for his contributions to the design and construction of much of the other electrical test apparatus.

References

[1] M. Fincke-Keeler, R. Keeler, and M. Lefebvre; *Performance Requirements of the Signal Feedthrough Vacuum Cables*, **ATL-AE-EN-0002**, Jun 1999.

[2] M. Fincke-Keeler and M. Lefebvre; *A proposal for a Low Voltage Cable Design for the HEC Feedthroughs in the ATLAS Endcap Cryostat*, ATLAS Internal Note **HEC 068**, Dec 1998.

[3] M. Fincke-Keeler, M. Lefebvre, and P. Poffenberger; *Cabling of the Endcap Signal Feedthroughs*, ATLAS Internal Note **ATL-AE-AN-0001/0002**, Nov 2000.

[4] P. Birney, A. Dowling, A.S. Dowling, M. Fincke-Keeler, T. Hodges, F. Holness, T. Ince, R. Keeler, R. Langstaff, M. Lefebvre, M. Lenckowski, J. Lindner, R. MacDonald, R. McDonald, E. Muzzeral, P. Poffenberger, J. Van Uytven, G. Vowles, and W. Wiggins; *ATLAS Endcap Signal Feedthrough Quality Assurance and Quality Control Document*, ATLAS Internal Note **ATL-AE-QA-0002 v.5** , Mar 2002.